Deep-Sea Research I 56 (2009) 1077–1092

Contents lists available at ScienceDirect

Deep-Sea Research I

journal homepage: www.elsevier.com/locate/dsri

# Long-term variation in the anticyclonic ocean circulation over the Zapiola Rise as observed by satellite altimetry: Evidence of possible collapses

Martin Saraceno [a,b,*], Christine Provost [c], Uriel Zajaczkovski [b,d]

[a] Centro de Investigaciones del Mar y la Atmósfera (CIMA), Intendente Güiraldes 2160, Ciudad Universitaria, Pab. II, 2do piso, Ciudad de Buenos Aires C1428EGA, Argentina

[b] Departamento de la Atmósfera y los Océanos, FCEyN, Universidad de Buenos Aires, Intendente Güiraldes 2160, Ciudad Universitaria, Pab. II, 2do piso, Ciudad de Buenos Aires C1428EGA, Argentina

[c] Laboratoire d'Océanographie et du Climat: Expérimentation et Approche Numérique (LOCEAN), Université Pierre et Marie Curie, Tour 45/55, 5ème étage, Boîte 100, 4 Place Jussieu, 75252 Paris cedex 05, France

[d] Departamento de Oceanografía, Servicio de Hidrografía Naval, Av. Montes de Oca 2124, Ciudad de Buenos Aires C1270ABV, Argentina

ARTICLE INFO

*Article history:*
Received 8 October 2008
Received in revised form
3 March 2009
Accepted 11 March 2009
Available online 26 March 2009

*Keywords:*
Zapiola Rise
South Atlantic circulation
Interannual variability

ABSTRACT

The Zapiola Rise (ZR) is a singular sedimentary deposit about 1200 m in height and 1500 km in width located in the Argentine Basin. In situ and satellite observations have revealed the presence of an intense counterclockwise circulation around the feature, with a volume transport comparable to those of the major ocean currents. The existence of a very low-frequency variability of the transport associated with the anticyclonic circulation is documented for the first time. As the Zapiola anticyclonic circulation plays a significant role in the mixing of the strongly contrasted water masses of the South Atlantic, variations in the anticyclonic transport can have a major impact on the mixing, hence a role in global climate variability. The circulation was clearly anticyclonic in the periods 1993–1999 and 2002–2007. In contrast, the 1999–2001 period did not show evidence of an anticyclonic flow in the mean surface velocity field. Moreover, the analysis of the weekly fields during that period of time revealed a cyclonic pattern from time to time. Previous work has shown that the flow can be considered as purely barotropic over the ZR region. A 15-year time-series of the transport was produced using absolute altimeter-derived geostrophic velocities. The estimated transport presents high-frequency variability associated with mesoscale activity superimposed on a low-frequency signal. The amplitude of the estimated transport is in good agreement with the only in situ-derived estimation available (80 Sv, January 1993). The low-frequency signal presents a minimum during the period 1999–2001, further suggesting that at times the Zapiola anticyclonic flow may have significantly decreased in strength or even vanished. Possible causes of the low-frequency variability are discussed.



## 1. Introduction

The Zapiola Rise (ZR) is a sedimentary elevation about 1200 m in height located in the Southwest Atlantic (Fig. 1). Its extent is roughly 1500 km in the east–west direction and 400 km in the north–south direction. The crest of the elevation extends in the east–west direction along 45°S with its summit (at 4900 m depth) centered at 45°S, 45°W.

* Corresponding author at: Centro de Investigaciones del Mar y la Atmósfera (CIMA), Intendente Güiraldes 2160, Ciudad Universitaria, Pab. II, 2do piso, Ciudad de Buenos Aires C1428EGA, Argentina.
*E-mail address:* saraceno@cima.fcen.uba.ar (M. Saraceno).

0967-0637/$ - see front matter © 2009 Elsevier Ltd. All rights reserved.
doi:10.1016/j.dsr.2009.03.005

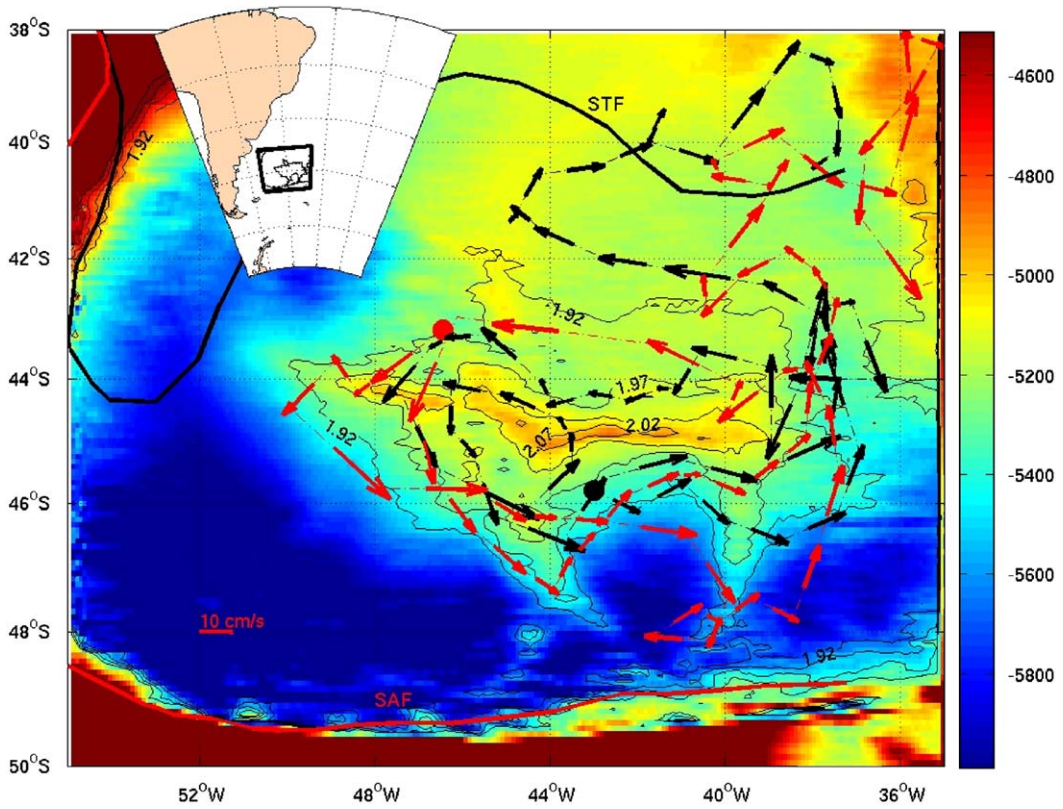


**Fig. 1.** Colors indicate the bathymetry in the Argentinean Basin between 4500 and 6000 m depth. Thin black lines indicate f/H isocontours (units $-1\times10^{-8}\,m^{-1}\,s^{-1}$). The closed contours range from $-2.1\times10^{-8}$ to $-1.92\times10^{-8}\,m^{-1}\,s^{-1}$. The mean positions (Saraceno et al., 2004) of the Subtropical Front (STF) and the Subantarctic Front (SAF) are indicated by solid black and solid red lines, respectively. The positions of these two fronts correspond, also respectively, to the southern limit of the South Atlantic Current and to the northern limit of the Antarctic Circumpolar Current. Vector speeds estimated from the trajectories of profilers pf3900111 (red arrows) and pf3900110 (black arrows) are indicated. The profiler starting points are indicated by solid dots. The vector scale (bottom-left corner) is common to both profilers. (For interpretation of the references to color in this figure legend, the reader is referred to the web version of this article.)

The rise is in the middle of the abyssal plain of the Argentine Basin, which is deeper than 5800 m south and west of the ZR and between 5400 and 5000 m depth north and east of the elevation. The local potential vorticity field ($f/h$) is influenced by this topographic feature and exhibits closed contours with minimum values around the summit (Fig. 1).

Several in situ observations reveal the presence of an anticyclonic circulation around the ZR. First, Flood and Shor (1988) suggested that the orientation of the mud waves present all around the ZR indicated that a strong anticyclonic circulation near the ocean floor existed for many thousands of years. Later, near-bottom current measurements (Weatherly, 1993; Whitworth et al., 1991) confirmed high near-bottom velocities compatible with an anticyclonic circulation. Saunders and King (1995a) estimated a nearly barotropic anticyclonic flow as strong as 100 Sv around the ZR, using data from a section of the World Ocean Circulation Experiment (WOCE) that crossed the ZR from east to west.

Evidence of the anticyclonic circulation around the ZR can also be observed with satellite altimetry. The ZR region appears as a local minimum in sea-surface-height variability, surrounded by very high values, up to 35 cm, typical of the mesoscale field of the Brazil-Malvinas Confluence (BMC) (de Miranda et al., 1999; Saraceno et al., 2005). Satellite altimetric data enabled the investigation of the intra-seasonal variability and evidenced a counterclockwise rotating dipole with a periodicity of 25 days centered near the ZR summit (Fu et al., 2001; Tai and Fu, 2005). This mode has been confirmed by a 2-year-long data set from bottom-pressure recorders (BPR) deployed in the region (Hughes et al., 2007). Eddy-propagation velocities computed from altimetric data exhibit a striking pattern around the ZR: eddies propagate along the path of the mean circulation at a speed comparable to that of the mean flow (Fu, 2006).

Other types of satellite data also show characteristic signals over the ZR. The amplitude of the sea-surface temperature (SST) gradient exhibits a minimum above the ZR (Saraceno et al., 2004). Combining monthly climatologies of SST, SST gradient and satellite-derived chlorophyll-*a* concentration, and using different methods, Saraceno et al. (2005, 2006) showed that the ZR region appears as a distinct biophysical region.

The Zapiola anticyclone (ZA) is thought to contribute significantly to the South Atlantic's interocean exchanges and its water-mass transformations (Garzoli et al., 2008).

It enhances the meridional exchange between the South Atlantic Current (40°S) and the Antarctic Circumpolar Current (48°S) as they cross the Argentine Basin (Fig. 1), as pointed out by Smythe-Wright and Boswell (1998) using tracers and by Boebel et al. (1999) using trajectories of neutrally buoyant floats. However, little is known about the temporal variability of the meridional exchange, probably because of a paucity of in situ data. The objective here is to investigate the long-term variability of the circulation associated with the ZR, using satellite altimeter data. Satellite data currently provide a time-series longer than 15 years, enabling some insight to be gained on the low-frequency variability of the sea-surface height (SSH) and the associated geostrophic currents. Previous studies (Saunders and King, 1995a; Fu, 2006; Hughes et al., 2007; Volkov and Fu, 2008) suggest that the flow can be considered as purely barotropic over the ZR region. Therefore, it is possible to assume a constant vertical profile of horizontal velocity and to use satellite altimetry data to compute the transport.

The article is organized as follows: the data used (i.e. satellite sea-level anomaly (SLA), ARGO profilers, surface drifters, and the hydrographic data from the World Ocean Circulation Experiment (WOCE) cruise A11) are presented in Section 2. A comparison between the geostrophic velocities estimated from (i) SLA satellite data; (ii) the trajectories of two ARGO profilers deployed in the region in 2002, and (iii) data collected along the WOCE A11 section follows (Section 3). The interannual variability of the surface circulation derived from altimetric data and from surface drifters is shown in Section 4. A transport time-series based on the SLA satellite data is presented in Section 5, followed by a discussion on the possible sources of the observed low-frequency variability (Section 6).

## 2. Data used

### 2.1. Satellite sea-level anomaly and mean dynamic topography

Satellite altimetry has revolutionized the field of physical oceanography since the launch of the TOPEX/Poseidon satellite in 1992 (Fu and Cazenave, 2001). We downloaded weekly, from the Aviso web site (ftp://ftp.cls.fr), the updated version of the gridded SLA data (at one-third of a degree resolution) produced by Ssalto/Duacs. The processing of along-track data from the altimetric missions of TOPEX/Poseidon, Jason-1, ERS-1, ERS-2 and Envisat into gridded fields of SLA is described in Le Traon et al. (2003). We extracted the SLA for the region of interest (60°W–35°W, 50°S–35°S) from the global SLA fields for the period 1993–2007 (15 years). AVISO SLA fields are computed with reference to a mean for the period 1993–1999. To avoid any spurious interannual variability, the temporal mean estimated for the whole time period considered was subtracted at each data point. Each field of SLA was then added to the mean dynamic topography (MDT) field estimated by Rio et al. (2005), to produce maps of absolute dynamic topography (MADT). The MDT produced by Rio et al. (2005) is a combined product based on the Gravity Recovery and Climate Experiment (GRACE) mission, altimetry and in situ data (hydrographic and drifter data). The geostrophic relationship was used to produce weekly absolute velocity fields for each MADT, conserving the one-third of a degree spatial resolution.

### 2.2. Argo profilers

The ARGO (Array for Real-time Geostrophic Oceanography) program is a common initiative of the CLIVAR (Climate Variability and Predictability) and GODAE (Global Ocean Data Assimilation Experiment) joint programs of the World Meteorological Organization and Intergovernmental Oceanographic Commission. The primary objective of ARGO is to obtain vertical profiles of temperature ($T$) and salinity ($S$) of the ocean for climate applications. At present, more than 3000 profilers are collecting $S$ and $T$ observations around the world ocean (http://www.usgodae.org/argo/argo.html). Each profiler has a mean lifetime of almost 5 years. The typical cycle of a profiler lasts 10 days. At the beginning of the cycle the profiler dives to the parking depth (usually 1500 or 2000 m), then it drifts during a given time (around 9 days) and then rises to the sea surface, measuring $T$ and $S$ during its ascent (6 h). Once at the surface, the profiler transmits several times its position, date and time and the data collected during the ascending cycle to a land reception base via satellite transmission. Data are then submitted for quality control and freely redistributed via the World Wide Web (see the previous link or http://www.coriolis.eu.org/). The position, date and time can be used to estimate the 10-day mean trajectory and speed of the profiler at the parking depth (Ichikawa et al., 2002). A rough approximation of the speed of the profiler can be obtained assuming a linear trajectory between two successive positions. The error due to the unknown drifts at the surface, during the ascent and the descent phases lies between 10% and 25% of the estimated mean current velocity (Ichikawa et al., 2002).

Two Argo profilers (pf3900110 and pf3900111) trapped in the circulation associated with the ZR for more than a year are examined here (Figs. 1 and 2). The two Argo profilers were launched on 15 and 17 May 2003 above the ZR and programmed to drift at a 1500-db parking depth.

### 2.3. WOCE A11 section

Section A11 of the international WOCE program was carried out between 22 December 1992 and 1 February 1993; it crossed the western South Atlantic from west to east (Saunders et al., 1993). The section went over the ZR along 45°S and measured $T$ and $S$ at hydrographic stations from the surface to the bottom of the ocean. In addition, a VM-ADCP (vessel-mounted acoustic doppler current profiler) measured velocity profiles in the upper 300 m of the water column (Saunders and King, 1995a). Geostrophic velocities estimated from the hydrographic station data and surface currents measured by the VM-ADCP are

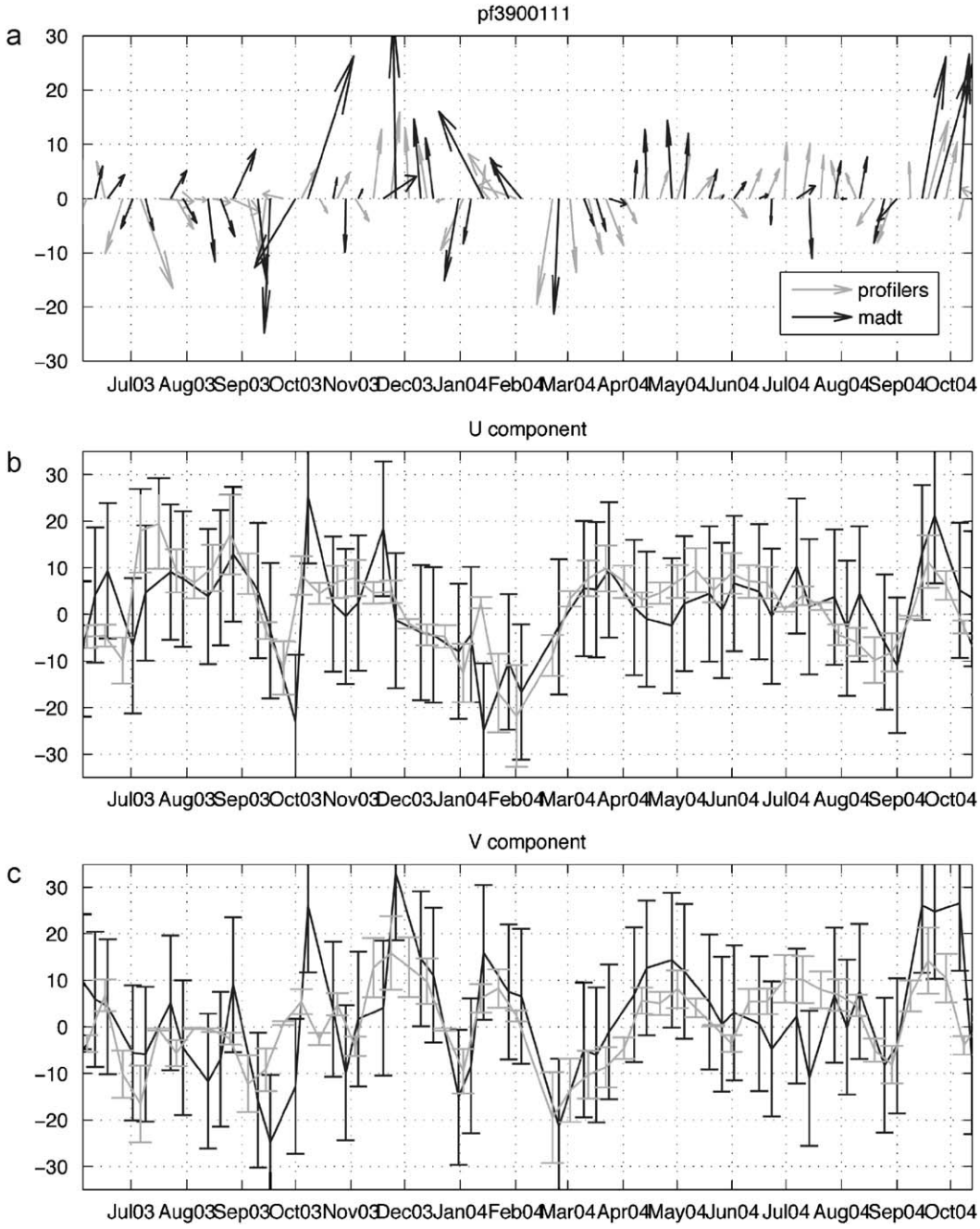


**Fig. 2.** Comparison between the vectors (panel a) and each of the components (zonal component, panel b; meridional component, panel c) obtained by the profiler pf3900111 (gray) and by altimetry (black). On (b) and (c), error bars are indicated.

compared with the geostrophic velocities obtained from the MADT (Fig. 3).

### 2.4. Satellite-tracked surface drifters

The satellite-tracked drifter data set used in this work is part of the global data set available from the Drifter Data Assembly Center (DAC) at the National Oceanographic and Atmospheric Administration's Atlantic Oceanographic and Meteorological Laboratory (AOML). The data set is public and can be downloaded from AOML's ftp server (ftp://ftp.aoml.noaa.gov).

Quality control at DAC involves the interpolation of the raw fixes (16–20 satellite fixes per day per drifter) to uniform six-hour intervals using a Kriging interpolation scheme (Hansen and Poulain, 1996). The data from drifters with no drogue attached were discarded, as well as all

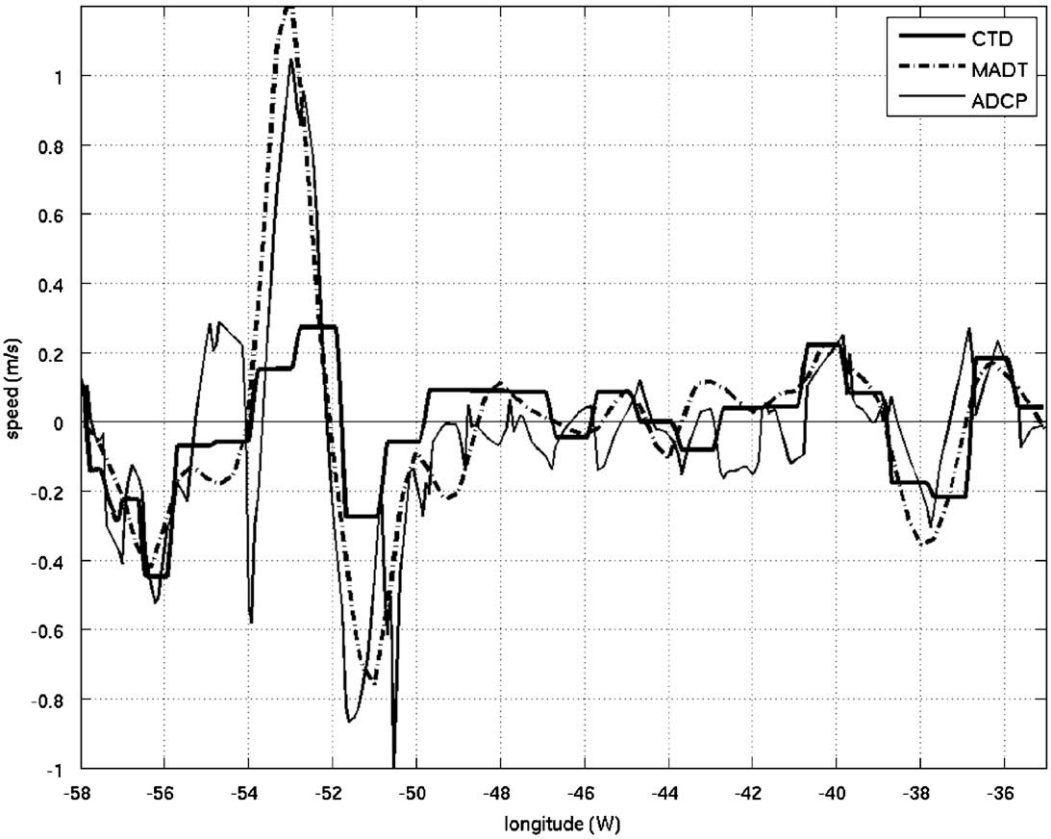


**Fig. 3.** Meridional component of the geostrophic velocity along 45°S obtained from the CTD data of the WOCE A11 section (bold line), MADT (dash-dotted line) and VM-ADCP at 30 m depth (thin line). Geostrophic velocities were computed using a zero velocity reference (the sea floor).

interpolated positions with an uncertainty greater than 1 km. The remaining trajectories were low-pass filtered with a 2-day Gaussian filter in order to remove tidal fluctuations and other high-frequency variability of no interest in the present study. The Ekman component, estimated following Ralph and Niiler (1999), was explicitly not included: at the latitude of the ZR the estimated Ekman velocity is similar to the velocity uncertainty (below 1 cm/s, even with strong winds).

## 3. Comparison of altimeter-derived geostrophic velocities with in situ current estimates

The results of the present work critically depend upon the quality of the altimeter-derived velocities. Therefore, our first concern is to compare the latter with independent velocity estimates. We compared the altimetric geostrophic velocities with the velocities estimated from the WOCE A-11 section and with those estimated from the ARGO profilers.

Comparison between altimeter-derived velocities and ARGO-derived velocities indicated a good agreement between the two different measurements (Fig. 2a). Since the comparison is between two vector time-series, we estimated the correlation between the two vector time-series using the vector correlation coefficient (VCC) (Crosby et al., 1993). The VCC between profiler pf3900111 and pf3900110 and the corresponding best time-matching velocities derived from MADT are 0.6 and 0.5, respectively (significant at 95% confidence level, CL). Correlations between single velocity components show a similar result: there are no significant differences between profilers and altimeter-derived velocities (Fig. 2b and c). Considering the time-space interpolations associated with the MADT and the errors inherent in velocity estimates based on the drift of ARGO floats, the agreement between velocities is very high. Since the parking depth of the ARGO floats is 1500 m and the altimeter-derived velocities are representative of the surface velocities, the above coefficients of correlation suggest that the vertical profile of velocities may be constant between the surface and 1500 m depth.

The RRS Discovery cruise passed over the Zapiola Rise between 2 and 7 January 1993 (Saunders et al., 1993); therefore, only the altimetrically derived image of geostrophic velocities centered on 6 January 1993 was considered for the comparison. Fig. 3 shows the meridional component of the velocities along 45°S estimated from: (i) the VM-ADCP of the WOCE A11 section; (ii) WOCE A11 hydrographic data; and (iii) the altimetrically derived geostrophic velocities. Velocities estimated from

hydrographic data represent only the baroclinic component of the flow. VM-ADCP and satellite-derived velocities contain both the barotropic and baroclinic signals and therefore can fairly be compared. Correlations and standard deviation of the difference (Table 1) show a good agreement between the geostrophic velocities estimated from satellite data and the VM-ADCP currents. To quantify which percentage of the total (barotropic plus baroclinic) current the baroclinic component represents, we followed Saunders and King's (1995a) procedure: the barotropic component is estimated as the difference between the VM-ADCP and the hydrographic velocities, both evaluated at 200 m depth, so as to avoid the mixed layer. CTD data were referenced to 4000 m depth, which corresponds to the limit between North Atlantic Deep Water and Lower Circumpolar Deep Water (Reid, 1989). Fig. 4 shows the amplitude of the baroclinic and barotropic components. On average, over the ZR, the baroclinic component represented only 23.8% of the sum of both components. This result agreed with observations by other authors (Saunders and King, 1995a; Hughes et al., 2007; Fu, 2006; Volkov and Fu, 2008) who concluded that the barotropic component is predominant over the ZR.

**Table 1**
Standard deviation of the differences between CTD, VM-ADCP and MADT velocities along the WOCE A11 section.

| | rms (cm/s) |
|---|---|
| CTD – VM-ADCP | 25 |
| CTD – MADT | 23 |
| VM-ADCP – MADT | 19 |

Saunders and King (1995a) computed the barotropic component in order to estimate the bottom currents along the section. They estimated the error estimate to 18 cm/s, and almost all the velocity estimates over the ZR are smaller than the error estimate. However, considering the good agreement that we obtained between the VM-ADCP and altimetric data, we assume here that the geostrophic velocities estimated from altimetry are representative of the mean depth-averaged currents around the ZR.

The above results encouraged us to estimate the transport associated with the ZR based on the altimetrically derived velocities and to consider a vertical profile of constant velocities. The transport calculation and results obtained are detailed in Section 5; surface velocities are presented in the following section.

## 4. Interannual variability of surface circulation

Fig. 5 shows the average of the altimeter-based geostrophic circulation around the ZR for different time periods. The mean circulation for the period 1993–1998 (Fig. 5, top panel) is similar to that for 2002–2007 (Fig. 5, bottom panel). Both periods featured an anticyclonic pattern centered at 44.5°S, 44.5°W, with a radius of about 150 km. The center of the swirl coincided with the top of the ZR. A larger anticyclonic pattern all around the ZR was

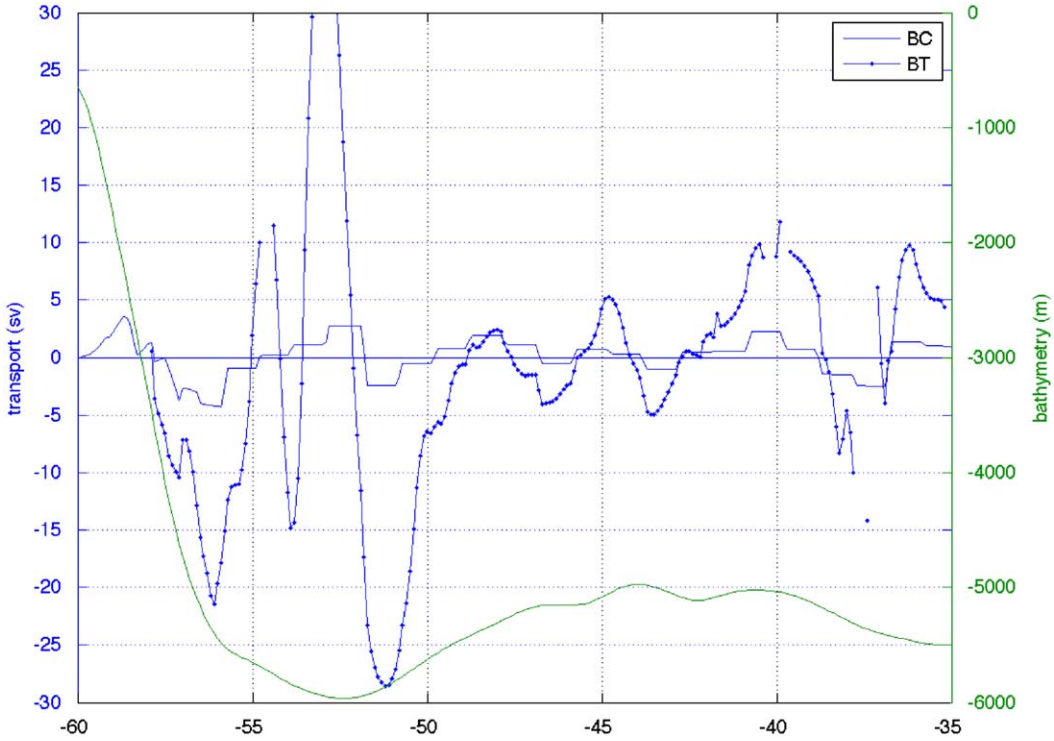


**Fig. 4.** Barotropic vs. baroclinic transport along WOCE A11 section. Barotropic transport (BT) is estimated using the bottom velocity (difference between S-ADCP and CTD velocities at 200 m depth, see text); baroclinic transport (BC) is estimated from CTD geostrophic velocities. Bathymetry (green line) is indicated for reference. (For interpretation of the references to color in this figure legend, the reader is referred to the web version of this article.)

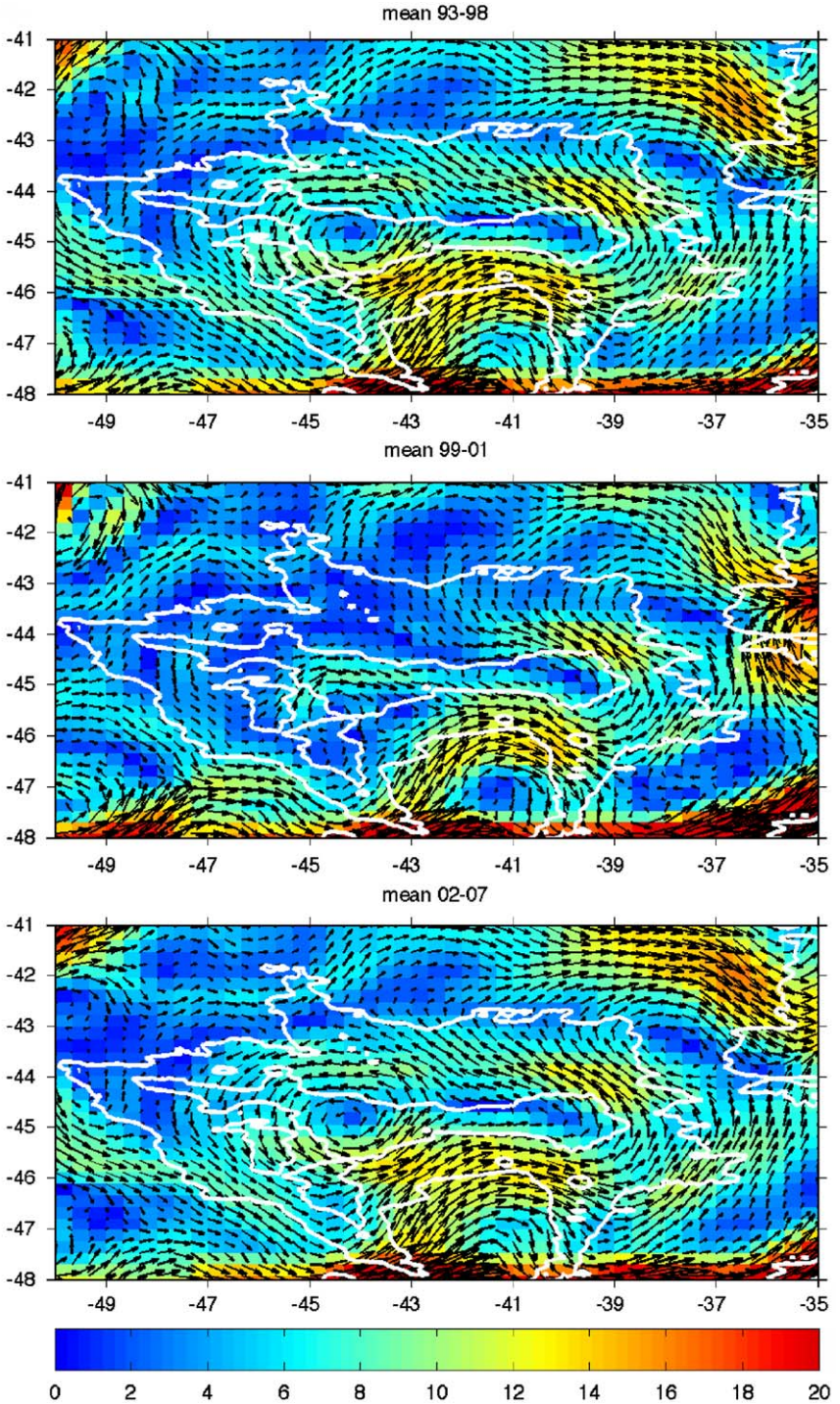


**Fig. 5.** Average of the absolute geostrophic currents for different time periods: 1993–1998 (upper panel), 1999–2001 (middle panel) and 2002–2007 (bottom panel). Vectors scale and color limits are the same for the three panels. Colors represent intensity of mean velocity (cm/s). The largest vectors in the figure represent velocities of 61 cm/s. White lines correspond to the closed potential vorticity contours $-1.92\times10^{-8}$ and $-2\times10^{-8}\,m^{-1}\,s^{-1}$. (For interpretation of the references to color in this figure legend, the reader is referred to the web version of this article.)

enclosed by the $-1.92\times10^{-9}\,m^{-1}\,s^{-1}$ potential vorticity contour. In contrast, the mean circulation for the 1999–2001 period (Fig. 5, middle panel) features an eastward zonal current near 45°S over the top of the ZR. East of 42°W the circulation pattern was similar during the three time periods.

The mean surface circulation estimated from surface drifters for the same time periods is displayed in Fig. 6.

The mean surface circulation was estimated using a cell size of 1 degree square. The choice of the spatial resolution was a compromise between the resolution needed to adequately depict the circulation and the constraint of having at least 10 observations per cell. Probably, because of this constraint, the anticyclonic swirl centered over the top of the ZR and roughly limited in the region 43°S–46°S and 43°W–45.5°W is not observed in Fig. 6. The amount of data is particularly low for the period 1999–2001 and probably biased the resulting circulation. However, a larger anticyclonic circulation can be inferred inside the $-1.92\times10^{-8}\,m^{-1}\,s^{-1}$ potential vorticity contour, somewhat similar to the circulation observed in Fig. 5.

In order to further investigate the interannual variability we constructed a time-series of the absolute geostrophic velocities and of the transport associated with the ZR. The former is examined below and the latter is analyzed in the next section. Both time-series are computed across four sections with a common origin at 44.5°S and 44.5°W (Fig. 7). The sections were chosen considering the closed contours of the MDT around the ZR. The four sections have their common origin at the center of the highest closed contour (143 cm) over the ZR and extend to the lowest contour (133.5 cm) that closes around the ZR. Since our goal is to estimate the transport around the ZR, only the mean values of the velocities along each of the sections are considered. To examine the low-frequency circulation associated with the ZR, a Loess (Cleveland and Devlin, 1988) low-pass filter (90-days 1/2 energy cut-off) was applied to each time-series. The non-filtered and 90-day low-pass-filtered time-series of the mean along each section are displayed in Fig. 8. To facilitate interpretation, the velocity values across the west and north sections were multiplied by −1, so the positive values for the four time-series in Fig. 8 correspond to a counterclockwise (anticyclonic) direction of flow. The four time-series show a maximum (significant at 99.5% CL) correlation at lag 0 (see Table 2), suggesting that, at low frequency, the fluid undergoes a quasi-'solid'

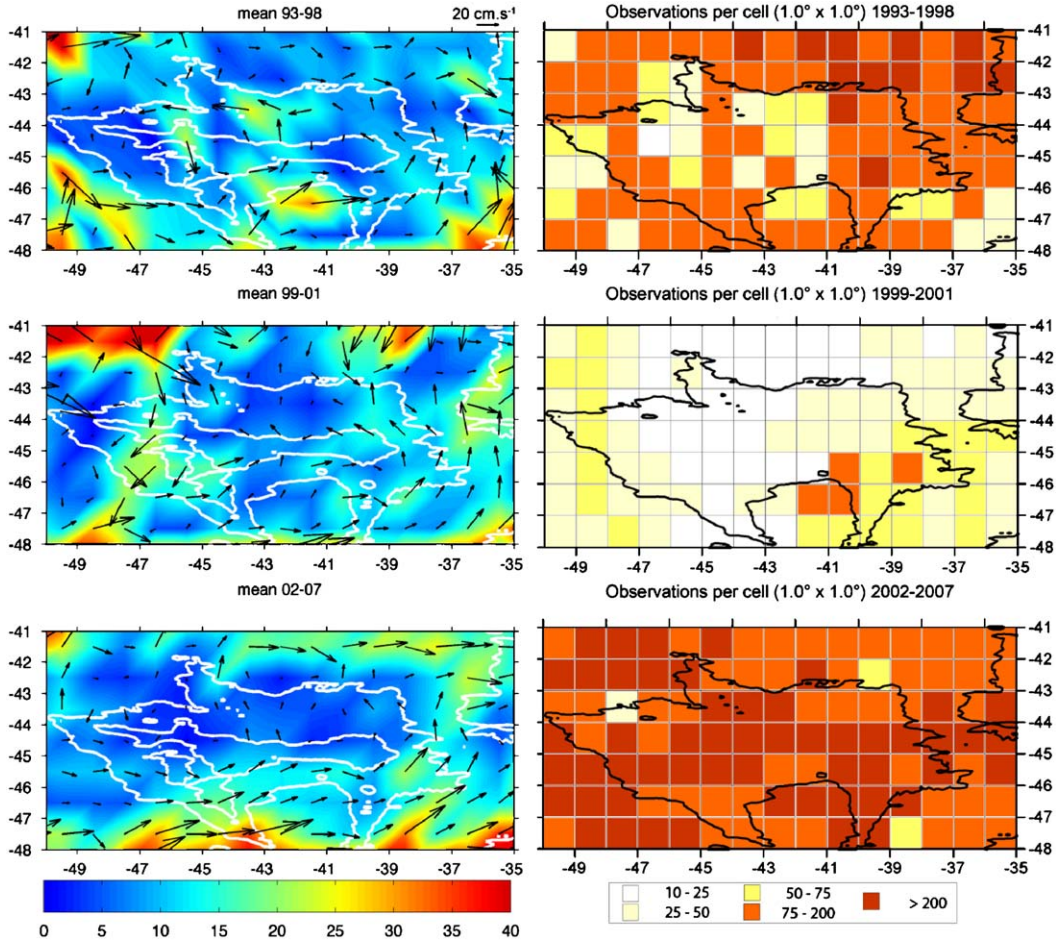


**Fig. 6.** Left column: Mean surface circulation estimated with satellite-tracked surface drifters for different time periods: 1993–1998 (upper panel), 1999–2001 (middle panel) and 2002–2007 (bottom panel). Colors represent intensity of mean velocity (cm/s). Right column: Observations per cell (bin size: 1.0 × 1.0°) corresponding to the three time periods considered. Potential vorticity contours are displayed as white lines on the left ($-1.92\times10^{-8}$ and $-2\times10^{-8}\,m^{-1}\,s^{-1}$) and with a black line ($-1.92\times10^{-8}\,m^{-1}\,s^{-1}$) on the right. (For interpretation of the references to color in this figure legend, the reader is referred to the web version of this article.)

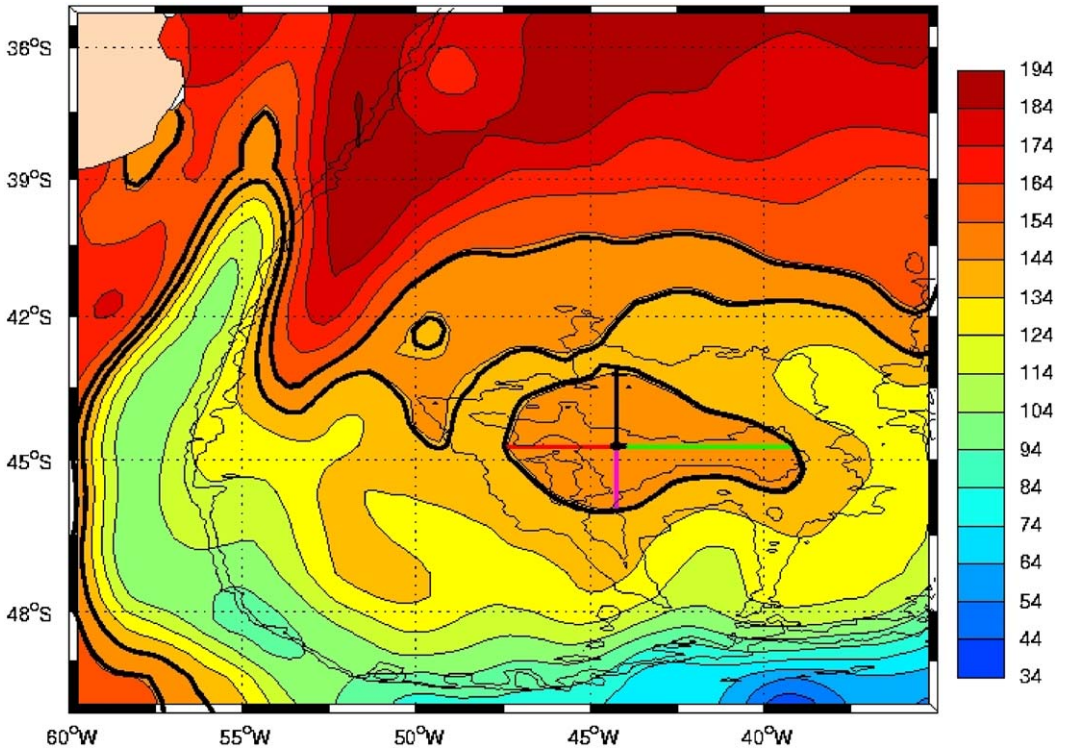


**Fig. 7.** Color-filled contours correspond to the mean dynamic topography (MDT) of Rio et al. (2005), in centimeters. Thick black lines show the highest (143 cm) and lowest (133.5 cm) closed MDT contours in the ZR region. Thin black lines correspond to the $-1.92\times10^{-8}$ and $-2\times10^{-8}\,m^{-1}\,s^{-1}$ potential vorticity isocontours. The straight thick magenta, red, green and black lines indicate, respectively, the south, west, north and east sections, which were considered to estimate the transport as a function of time. The four sections have their common origin at 44.5°W, 44.5°S. (For interpretation of the references to color in this figure legend, the reader is referred to the web version of this article.)

rotation. The standard deviation (SD) of the velocity time-series was maximum in the south and north sections (5.7 and 5.8 cm/s, respectively). The SDs for the west and east sections were 3.8 and 3.3 cm/s, respectively. This observation may suggest that higher variability is introduced into the ZA through the interaction with eddies from the northern and southern borders, rather than through the western and eastern borders. Possible sources of eddies are the overshoot of the BMC, the northern branch of the ACC and the South Atlantic Current, located, respectively, near the western, southern and northern limits of the ZA.

The mean, minimum and maximum of the four 90-day low-pass-filtered time-series are combined in Fig. 9a. The range of values that the velocity time-series can span at a given time (shaded region in Fig. 9a) provides a measure of how well organized is the flow at that particular time. For example, the flow was not so well organized during most of 1996, whereas a remarkable correspondence between the velocities along the sections was observed in January 2002 and December 2006.

The mean over the four sections of the low-frequency time-series (solid black line in Fig. 9a) spanned a large range of values, from 12 to −4 cm/s: while most of the time the mean velocity was positive, corresponding to the anticyclonic circulation, negative values for all the sections occurred during very short periods of time in mid-1999 and early-2001, suggesting a collapse of the anticyclonic circulation.

The 4.3-year low-pass-filtered time-series (dash-dotted line in Fig. 9a) suggests a low-frequency modulation of the mean velocity, with a minimum from January 1999 to December 2001 and maxima occurring early-1996 and mid-2005.

## 5. Transport estimates

To compute the transport we considered a constant vertical profile of velocities based on the surface geostrophic velocities. This choice was justified by the fact that the current velocities in the region can be considered as constant throughout the water column, as discussed in Section 3. Thus, transport time-series along the four sections were obtained multiplying the surface geostrophic velocities by the ocean depth. Depth was estimated using Smith and Sandwell (1994) bathymetry. We first estimated the mean transport along the four sections using only the MDT. Since the four sections were selected between the same closed contours of MDT, it is not surprising that the transport obtained was the same (about 50 Sv, $1\ Sv = 10^6\,m^3\,s^{-1}$) at any of the four sections. Then we estimated the time-series of the transport around the ZR along the same four sections described in the previous section (Fig. 9b). Velocity (Fig. 9a) and transport (Fig. 9b) time-series showed very similar variability, because we are considering constant vertical profiles to

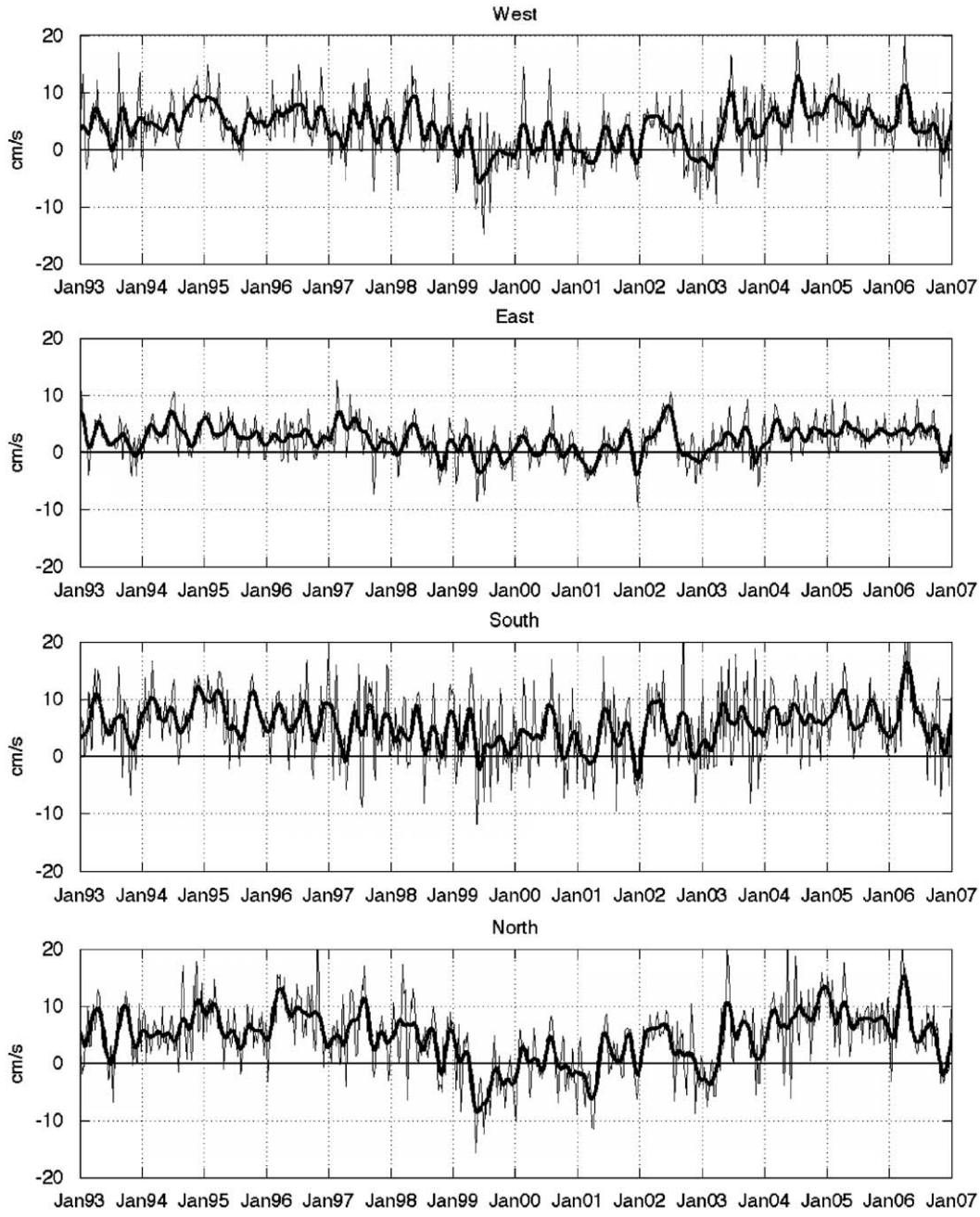


**Fig. 8.** Mean velocities (cm/s) along four sections that cross the Zapiola Rise. Sections are represented in Fig. 7. The meridional velocities are considered along the west and east sections and the zonal velocities along the north and south sections. The thin line represents the non-filtered mean and the bold line the 90-day low-pass-filtered mean. The east and north means are multiplied by −1, so positive values represent anticyclonic circulation.

estimate the transport. Differences among the four sections are due mainly to differences in the depth and length of the sections. Mean values were close to the values obtained considering only the MDT (50 Sv). This was expected because: (i) the geostrophic velocities were estimated from the sum of the SLA and the MDT; and (ii) the mean of the SLA is, by definition, null.

The 90-day low-pass-filtered time-series of the mean transport (bold solid line in Fig. 9b) spanned a large range of values, from −78 to 128 Sv. Most of the time the mean transport was positive, corresponding to an anticyclonic circulation. Negative values were found in all sections during relatively short periods of time, suggesting, as observed in the absolute geostrophic velocity time-series, a collapse of the anticyclonic circulation.

The 4.3-year low-pass-filtered transport time-series (dash-dotted line in Fig. 9b and c) suggests that the transport was modulated by a very low-frequency signal.

**Table 2**
Correlation coefficients at lag zero and corresponding confidence levels among the four time series shown in Fig. 8.

| Sections compared | Correlation | 99.5% Confidence level |
|---|---|---|
| W–E | 0.6285 | 0.5320 |
| E–S | 0.5614 | 0.4680 |
| S–N | 0.6556 | 0.5530 |
| N–W | 0.8348 | 0.6660 |
| W–S | 0.7085 | 0.5140 |
| E–N | 0.6418 | 0.5760 |

On each case the correlation is maximum at lag 0.

The length of the time-series (15 years) is a clear constraint in producing the 4.3 low-pass-filtered time-series, in particular near the boundaries relevant to the time-series. For this reason the very low-frequency signal obtained was superimposed on the yearly average of the transport in Fig. 9c. The filtered time-series follows the fluctuations depicted by the yearly average, providing some support to the very low-frequency signal hypothesis.

The transport estimates obtained in the present work were compared with estimates from other studies in the next section. In addition, to understand the nature of the low-frequency variability, we analyzed time-series of the wind stress curl and eddy kinetic energy.

## 6. Discussion

### 6.1. Accuracy of the estimated transport

Our estimations of the transport around the ZR can be compared with values obtained during the WOCE A11 cruise and with mean values derived from numerical models that were able to reproduce the ZA. Saunders and King (1995b) estimated a transport of 80 Sv associated with the ZA, using the hydrographic data collected on the WOCE A11 section in January 1993. The 90-day low-pass-filtered mean transport during January 1993 was 72 Sv (see Fig. 9b), in good agreement with Saunders and King's (1995b) estimate. However, the sections that we used were not the same as those used by Saunders and King (1995b). We used four sections (two zonal and two meridional) the limits of which were based on the largest and smallest closed contours of potential vorticity enclosing the ZR (Section 4). Saunders and King (1995b) arbitrarily established the ZA limits in a zonal direction, based on the structure of the meridional velocity fields encountered at the time of the WOCE cruise. Given the large sea-bed depth in the region (about 5 km), the choice of those limits strongly affects the transport estimate.

The few theoretical (Dewar, 1998) and numerical models (de Miranda et al., 1999; Volkov and Fu, 2008) that have successfully reproduced an anticyclonic pattern around the ZR found mean transport values of 100, 140 and 77.5 Sv, respectively. The first two values are significantly higher than our long-term mean of 50 Sv.

The transport obtained from satellite altimetric data depends upon the MDT used. We compared the MDT used in the previous section (Rio et al., 2005) with the one produced by Maximenko and Niiler (2005) (Fig. 10). Both MDTs have similar contours: the difference between the highest and lowest closed potential vorticity contours was 3.5 cm. Using Maximenko and Niiler's MDT leads to a mean transport of 40 Sv, which is 10 Sv lower than the mean transport estimated using the Rio et al. (2005) MDT. The relatively small difference between the two MDTs suggests either that the mean transport estimated by Dewar (1998) and de Miranda et al. (1999) overestimated the ZA transport or that it is not representative of the mean for the time period considered here (1993–2007). Volkov and Fu (2008) averaged their model outputs over almost the same time period (1993–2006) as that considered here, which is probably why their value is closer to the one obtained with the MDTs.

The mean and standard deviation (SD) of the altimeter-derived transport are of the same order of magnitude, the SD of the mean of the four non-filtered and 90-day-filtered time-series was 52 and 41 Sv, respectively. Using Maximenko and Niiler's (2005) MDT, the mean transport and associated SD decreased to 48 and 34 Sv, respectively. To our knowledge, these are the first SD estimates of the ZA transport; they reveal a high variability of the ZA circulation.

The low-frequency variability observed in the transport time-series corresponds to acceleration or deceleration of the main flow. A low-frequency variability of the ZA transport has been recently found in numerical simulations. Bigorre (2005) used the model described by Dewar (1998) and constructed a 200-year time-series of the transport associated with the ZR. His time-series showed a statistically significant peak (at 95% CL) centered at 6–7 years that is set by basin mode perturbations. The sensitivity to these perturbations is determined locally by the eddy field activity (Bigorre, 2005). Although periodicity of 6–7 years could also be suggested in the present work (Fig. 9b), the relatively short time span of the altimetric series (15 years) does not allow us to properly assess the nature of the low-frequency signal.

During the period 2004–2007, six ARGO profilers (profilers numbered 3900802, 3900603, 3900397, 3933900, 3900112 and 3900383) were trapped by the ZA consistently with the circulation estimated using satellite altimetry (figures not shown). No ARGO profilers were found over the ZR in the time period 1999–2001; i.e., when the satellite measurements suggested a minimum in the strength of the ocean circulation associated with the ZR.

### 6.2. Possible forcing mechanisms of the low-frequency variability

Dewar (1998) and Bigorre (2005) suggested that the eddy kinetic energy (EKE) is the main source of energy for the ZA. We investigated whether the low-frequency variability of the estimated transport time-series discussed in the preceding section and the EKE were correlated over the 15 years of the altimeter record. We first estimated the EKE for each single bin in the domain of

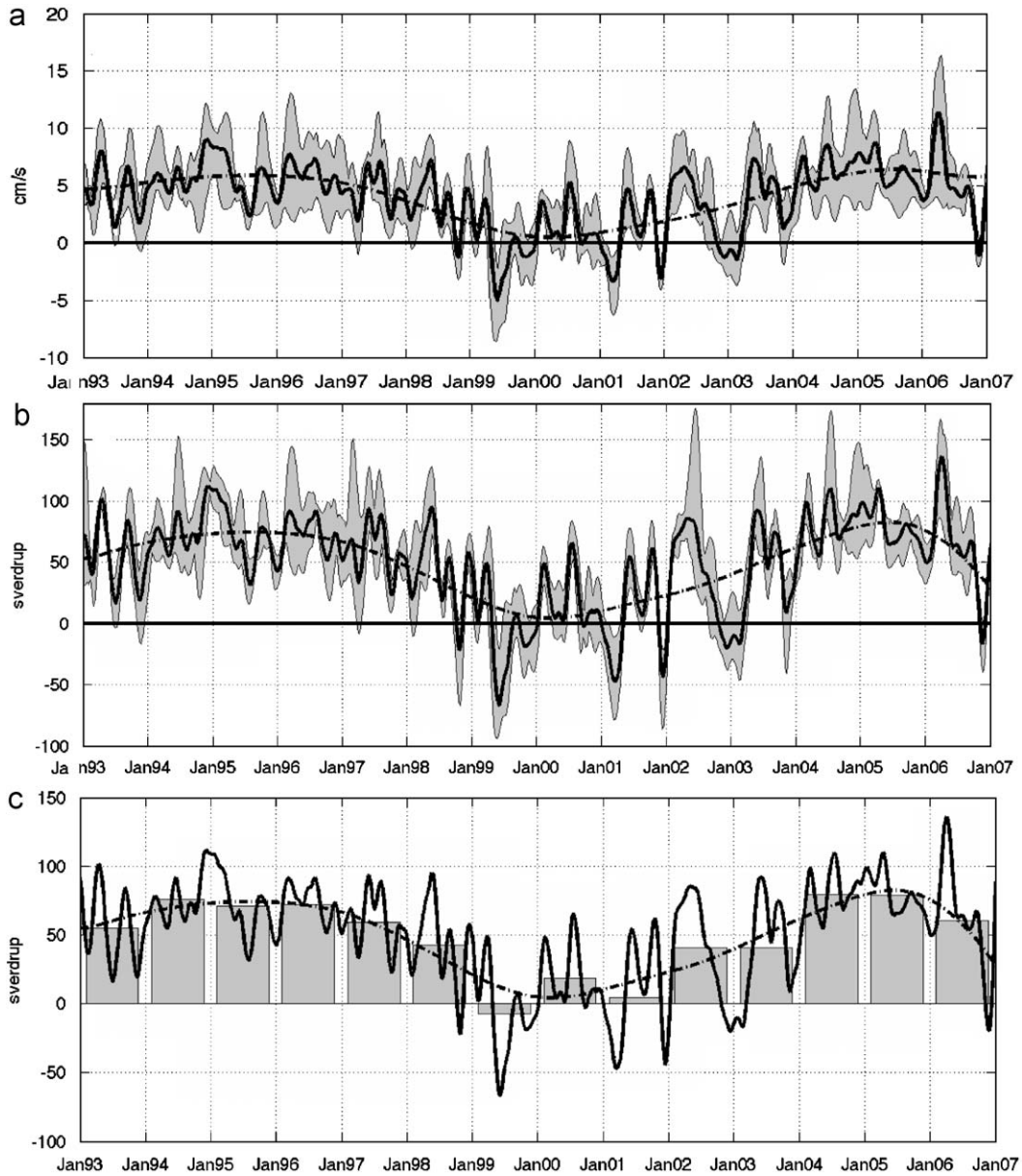


**Fig. 9.** (a) Absolute geostrophic velocity (cm/s) time-series obtained along the four sections indicated in Fig. 7. Values across the west and north sections were multiplied by −1, so that positive values for the four time-series suggest a counterclockwise (anticyclonic) direction of the flow. The vertical limits of the shaded region correspond to the minimum and maximum values in the four 90-day low-pass-filtered time-series. The average of the four 90-day low-pass-filtered time-series is indicated with a thick black line and the analogous average with a 4.3-year filter, by a dash-dotted line. (b) As in (a) but for the transport time-series. (c) As in (b), but without the shaded region and including on the background the yearly average of the mean transport (shaded boxes).

interest. Then we correlated each time-series of EKE with the transport time-series. We estimated the correlation with time lags ranging from −20 up to +20 weeks, thus obtaining 41 correlation-coefficient maps. The result, displayed in Fig. 11, corresponds to lag 0; only bins with a significant correlation at 95% CL or above are shown. A similar pattern was obtained for lags ranging from −3 to +3 weeks; this was expected since the transport time-series was low-pass-filtered at 90 days. Beyond that lag range, no regions with an area larger than 20 contiguous bins (approximately 28,000 $km^2$) having a significant correlation were found. At lag 0 (Fig. 11) a large region of significantly correlated bins (about 90,000 $km^2$) was found around the ZR. The region lies mostly between the maximum and minimum potential vorticity contours that enclose the ZR. Although a correlation does not establish a causal relationship between the variables analyzed, the above result supports Dewar's (1998) and Bigorre's (2005) suggestion that the EKE is the main driver of the ZA. Additionally, Fig. 11 shows that the region of higher

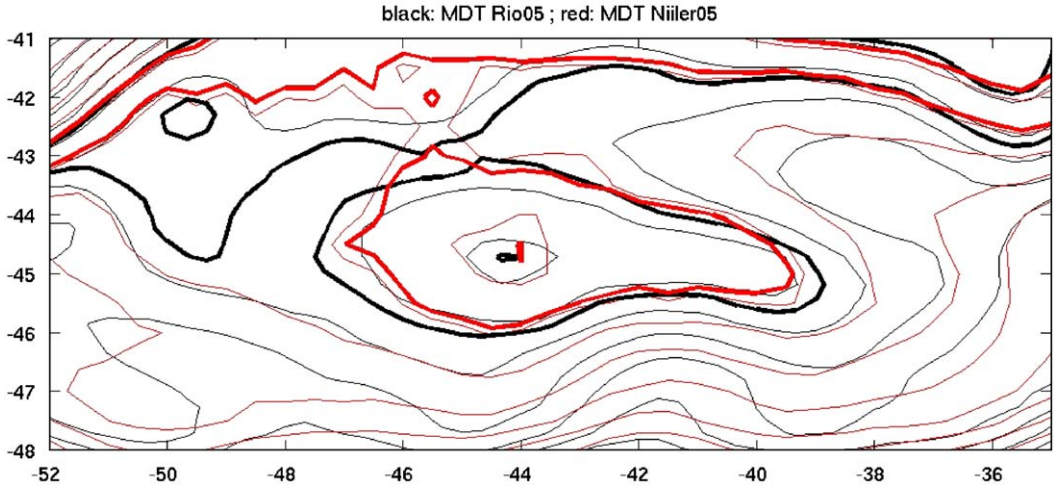


**Fig. 10.** Comparison of MDT: red lines correspond to Maximenko and Niiler (2005) and black lines to Rio et al. (2005). Bold contours correspond to the largest and smallest closed isolines around the ZR. (For interpretation of the references to color in this figure legend, the reader is referred to the web version of this article.)

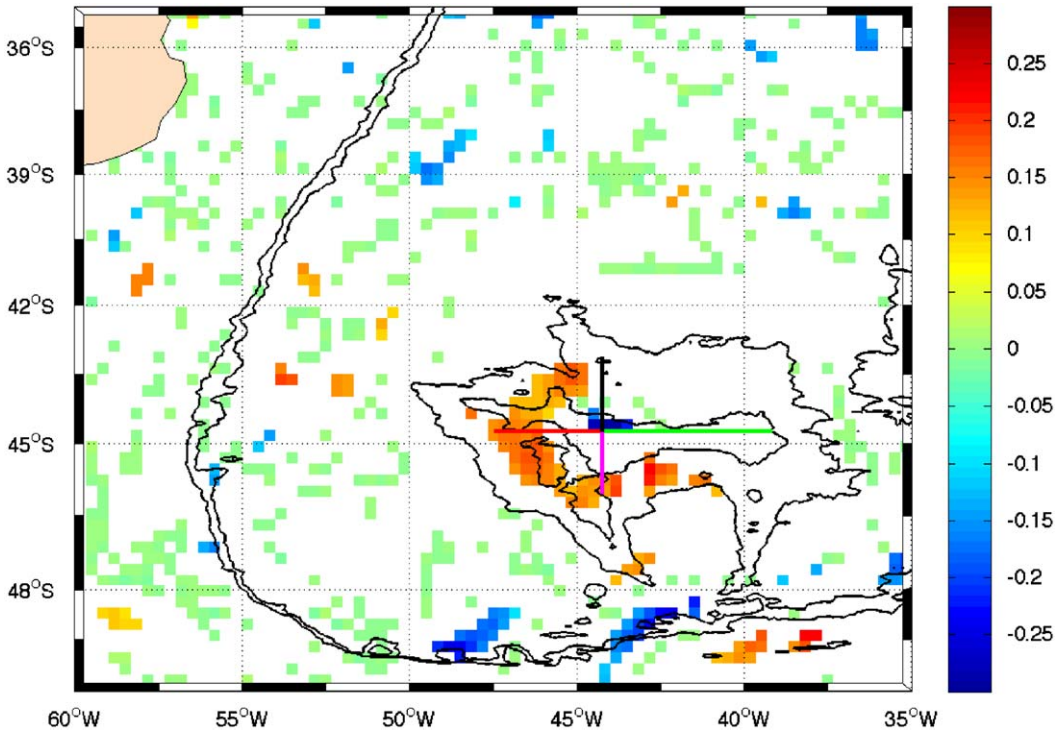


**Fig. 11.** Correlation coefficient at lag 0 between the transport time-series and the EKE obtained at each grid point. Only values that are above the 95% CL are shown. Contours of $f/h$ are reproduced as in previous figures.

interaction between eddies and the ZA is not everywhere around the ZR, but mostly at the southern and western boundaries of the ZA. This observation is consistent with the fact that the main sources of eddies that could affect the ZA are the northern branch of the Antarctic Circumpolar Current (ACC) (through the southern boundary) and the BMC (through the western boundary). Analyzing potential vorticity fluxes, Volkov and Fu (2008) also found that the northern branch of the ACC plays a major role in controlling the variability of the ZA.

To investigate possible sources of the interannual variability associated with the ZA, we plotted the time-series of the EKE averaged around the ZR versus the transport time-series (Fig. 12). The EKE time-series was constructed by averaging, at each time step, the EKE values in the bins where the EKE and the transport were

significantly correlated (Fig. 11). The maximum correlation (0.5) between EKE and ZA transport (significant at 95% CL) was at lag 0, suggesting a very rapid adjustment of the ZA to changes in the EKE. The 4.3-year low-pass-filtered EKE and transport time-series presented a minimum between January 1999 and December 2001 (Fig. 12). These results are consistent with view that the eddy field activity plays a major role in controlling the transport around the ZR.

Using the same data set of satellite altimetry used in the present work, Fu (2007) showed evidence of the interaction between the mesoscale activity and the large-scale (1000 km) 25-day-period waves trapped within the ZA. Considering the results presented in the present work, mesoscale activity is confirmed as the main forcing in the ZR region.

The low-frequency variability associated with the ZA may also be forced by low-frequency variability of the wind stress curl. We estimated the wind stress curl using (i) QuikScat scatterometer data (http://podaac.jpl.nasa.gov/quikscat) for the period October 1999–December 2006 and (ii) the NCEP reanalysis (www.cdc.noaa.gov) for the period January 1993–December 2006. To compare both wind data sets, we averaged the wind stress curl over a region that included the ZR (50°–36°W and 48°–39°S). Where the two time-series overlap, they agree very well (Fig. 13). This result is not surprising, since the NCEP reanalysis assimilated the satellite scatterometer data. We compared the NCEP wind stress curl time-series with the ZA transport time-series, regardless of the possibility that, for the period prior to the existence of the scatterometer, the NCEP data may be seriously biased (Chelton and Freilich, 2005). The time-series of the average of the wind stress curl does not present a significant correlation with the altimeter-derived ZA transport estimates (Fig. 14). The result seems to be independent of the domain shape and

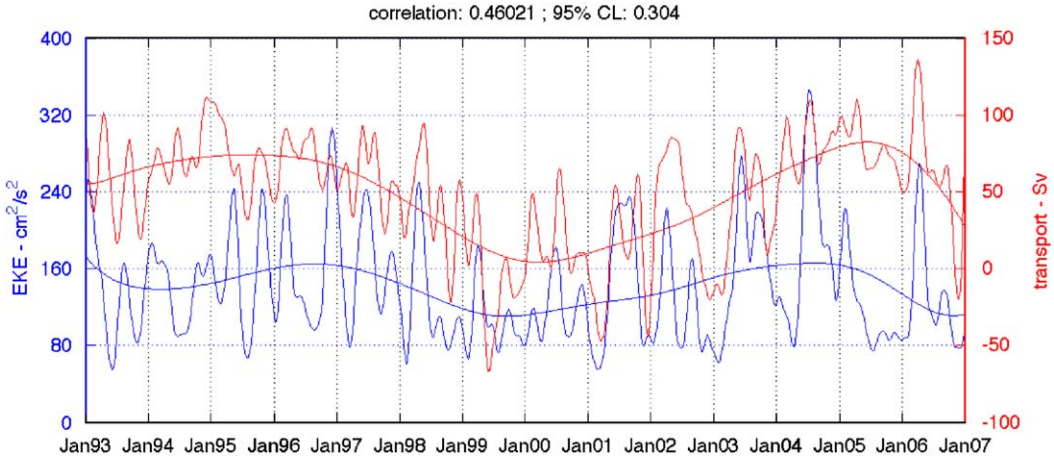


**Fig. 12.** Eddy kinetic energy (blue line) estimated in the border region of the ZR from SSH (see Fig. 10) and time-series of transport (red line), as estimated from altimetry. Both time-series are 90-day and 4.3-year low-pass-filtered. In the title the correlation between the 90-day low-pass-filtered time-series is indicated. (For interpretation of the references to color in this figure legend, the reader is referred to the web version of this article.)

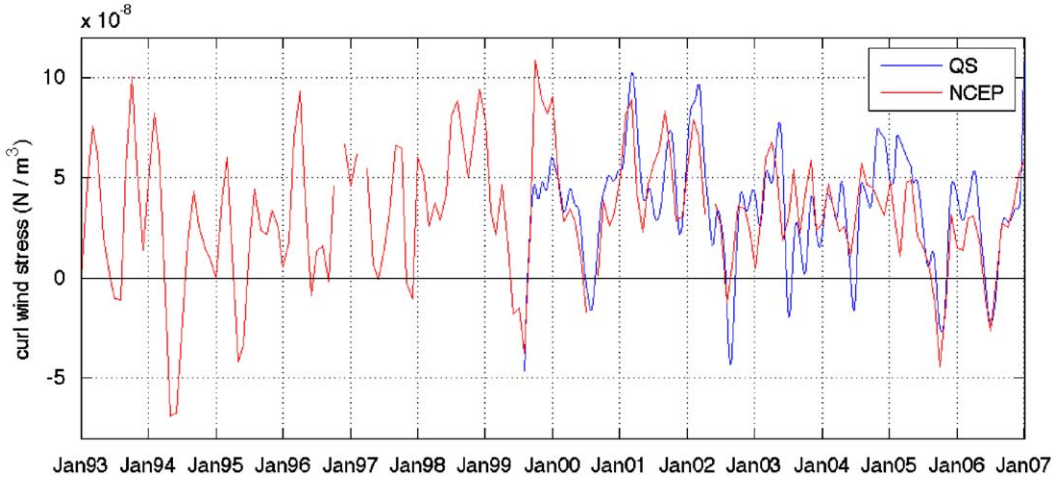


**Fig. 13.** Wind stress curl from NCEP reanalysis (red line) and from Quikscat (blue line) averaged over the ZR (between 50°–36°W and 48°–39°S). Correlation coefficient between both time-series is maximum at zero lag (0.72, significant at 99.9 CL). (For interpretation of the references to color in this figure legend, the reader is referred to the web version of this article.)

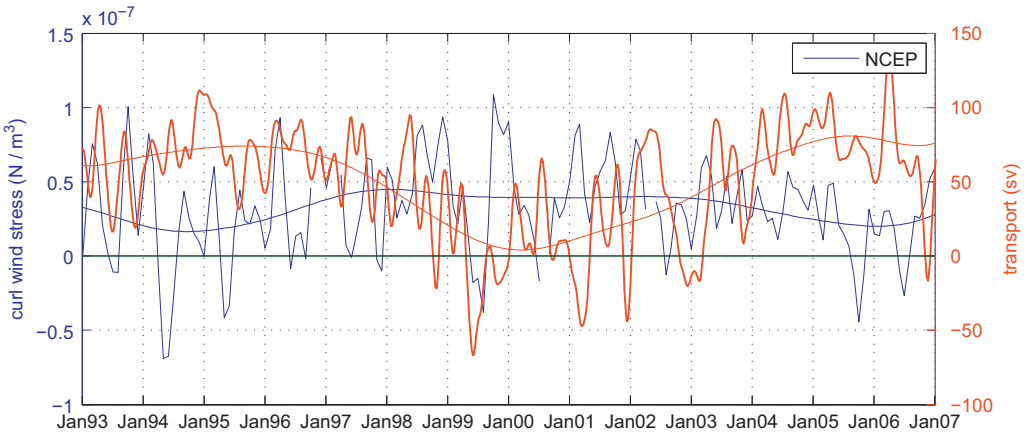


**Fig. 14.** Comparison between the NCEP wind stress curl and transport at the ZR. Both time-series are 90-days and 4.3-year low-pass-filtered.

size, provided that the ZR is contained in the domain considered (not shown). On the other hand, the 4.3-year low-pass-filtered time-series appears to be inversely correlated with the minimum in the transport time-series corresponding to a maximum in the wind stress curl (Fig. 14). Thus, the low-frequency variability of the ZA transport may be linked to changes in wind stress curl over the region. Hughes et al. (2007) analyzed the local wind stress curl in the region; they did not find a significant correlation with the data from two BPRs deployed over the ZR. However, since their time-series was only 1 year long, they were not able to detect a 4.3-year frequency. Though the wind stress curl does not seem to have a major impact on the variability of the ocean circulation in the region on short time-scales (seasonal or intra-seasonal), our results suggest that it may have an impact over larger periods of time, the dynamics of which are yet to be examined.

The ZA circulation contributes to the stirring of the strongly contrasted water masses in the western South Atlantic. Near the surface it promotes exchanges between the Antarctic Circumpolar Current and the South Atlantic Current (Smythe-Wright and Boswell, 1998). At depth, elements of the deep waters formed in the North Atlantic (as the North Atlantic Deep Water) encounter waters formed off the Antarctic Continent (as the Lower Circumpolar Deep Water or the Upper Circumpolar Deep Water), and the stirring associated with the ZA possibly constitute an important factor in determinating the characteristics of global deep water masses (Garzoli et al., 2008). A decrease in the intensity of the anticylonic flow, as suggested in the present study, could have a major impact on deep water mixing and thus play an important role in global climate variability. Further in situ observations are necessary to validate the amplitude of the transport variations and the vertical structure of the flow in this region.

## Acknowledgements

SLA products have been produced by Ssalto/Duacs in the framework of the Evironment and Climate EU (European) Enact Project (EVK2-CT2001-00117) and then distributed by AVISO, with CNES support (Centre National des Etudes Spatiales). We thank Bernard Barnier and Prof P.T. Strub for their valuable comments. MS and CP are grateful for the continuous CNES support. MS was supported by CONICET (Argentina) and Oregon State University. UZ was supported by grant from the Inter-American Institute for Global Change Research (IAI) CRN 2076 which is supported by the US National Science Foundation (Grant GEO-0452325).

## References

Bigorre, S., 2005. Topographic effects on wind driven oceanic circulation. Ph.D. Thesis, Florida State University, 100pp. Available on line at 〈http://etd.lib.fsu.edu/theses/available/etd-07052005-163825/unrestricted/pro-dis2E.pdf〉.

Boebel, O., Davis, R.E., Ollitrault, M., Peterson, R.G., Richardson, P.L., Schmid, C., Zenk, W., 1999. The intermediate depth circulation of the western South Atlantic. Geophys. Res. Lett. 26 (21), 3329–3332.

Chelton, D.B., Freilich, M.G., 2005. Scatterometer-based assessment of 10-m wind analyses from the operational ECMWF and NCEP numerical weather prediction models. Mon. Weather Rev. 123 (2), 409–429.

Crosby, D., Breaker, L., Gemmill, W., 1993. A proposed definition for vector correlation in geophysics: theory and application. J. Atmos. Oceanic Technol. 10, 355–367.

de Miranda, A.P., Barnier, B., Dewar, W.K., 1999. On the dynamics of the Zapiola Anticyclone. J. Geophys. Res. 104, 21137–21150.

Dewar, W.K., 1998. Topography and barotropic transport control by bottom friction. J. Mar. Res. 56 (2), 295–328.

Flood, R.D., Shor, A.N., 1988. Mud waves in the Argentine Basin and their relationship to regional bottom circulation patterns. Deep-Sea Res. Part A. Oceanogr. Res. Papers 35 (6), 943–971.

Fu, L.L., Cazenave, A., 2001. Satellite Altimetry and Earth Sciences, A Handbook of Techniques and Applications, International Geophysics Series, vol. 69. Academic Press, San Diego.

Fu, L.-L., Cheng, B., Qiu, B., 2001. 25-Day period large-scale oscillations in the Argentine Basin revealed by the TOPEX/Poseidon altimeter. J. Phys. Oceanogr. 31 (2), 506–517.

Fu, L.-L., 2006. Pathways of eddies in the South Atlantic Ocean revealed from satellite altimeter observations. Geophys. Res. Lett. 33, L14610.

Fu, L.L., 2007. Interaction of mesoscale variability with large-scale waves in the Argentine Basin. J. Phys. Oceanogr. 37, 787–793.

Garzoli, S.L., Piola, A.R., Speich, S., Baringer, M., Goni, G., Donohue, K., Meinen, C., Matano, R.P., 2008. A monitoring system for heat and mass transports in the South Atlantic as a component of the meridional overturning circulation. Workshop Report: Estancia San Ceferino, Buenos Aires, Argentina, 8–10 May 2007, 38pp, International CLIVAR Project Office, Southampton, UK (available at 〈http://eprints.soton.ac.uk/50121/〉).

Hansen, D.V., Poulain, P.-M., 1996. Quality control and interpolations of WOCE-TOGA drifter data. J. Atmos. Oceanic Technol. 13, 900–909.
Hughes, C.W., Stepanov, V.N., Fu, L.L., Barnier, B., Hargreaves, G.W., 2007. Three forms of variability in Argentine Basin ocean bottom pressure. J. Geophys. Res. 112 (C01011), 1–17.
Ichikawa, Y., Takatsuki, Y., Mizuno, K., Shikama, N., Takeuchi, K., 2002. Estimation of drifting velocity and error at parking depth for the ARGO float. Argo Technical Report, FY2001.
Le Traon, P.Y., Faugère, Y., Hernandez, F., Dorandeu, J., Mertz, F., Ablain, M., 2003. Can we merge GEOSAT follow-on with TOPEX/Poseidon and ERS-2 for an improved description of the ocean circulation? J. Atmos. Oceanic Technol. 20, 889–895.
Cleveland, W.S., Devlin, S., 1988. Locally weighted regression: an approach to regression analysis by local fitting. J. Am. Stat. Assoc. 83, 596–610.
Maximenko, N.A., Niiler, P.P., 2005. Hybrid decade-mean global sea level with mesoscale resolution. In: Saxena, N. (Ed.), Recent Advances in Marine Science and Technology, 2004. PACON International, Honolulu, pp. 55–59.
Ralph, E.A., Niiler, P.P., 1999. Wind-driven currents in the tropical Pacific. J. Phys. Oceanogr. 29 (9), 2121–2129.
Reid, J.L., 1989. On the total geostrophic circulation of the South Atlantic Ocean: flow patterns, tracers, and transports. Prog. Oceanogr. 23 (3), 149–244.
Rio, M.-H., Schaeffer, P., Lemoine, J.-M., Hernandez, F., 2005. Estimation of the ocean mean dynamic topography through the combination of altimetric data, in-situ measurements and GRACE geoid: from global to regional studies. In: Proceedings of the GOCINA International Workshop, Luxembourg.
Saraceno, M., Provost, C., Piola, A., 2005. On the relationship of satellite-retrieved surface temperature fronts and chlorophyll-*a* in the western South Atlantic. J. Geophys. Res. 110 (C11).
Saraceno, M., Provost, C., Lebbah, M., 2006. Biophysical regions identification using an artificial neuronal network: a case study in the southwest Atlantic. J. Adv. Space Res. 37 (4), 793–805.
Saraceno, M., Provost, C., Piola, A.R., Bava, J., Gagliardini, A., 2004. The Brazil Malvinas Frontal System as seen from nine years of AVHRR data. J. Geophys. Res. 109 (C5).
Saunders, P., King, B.A., 1995a. Bottom current derived from a shipborne ADCP on WOCE cruise A11 in the South Atlantic. J. Phys. Oceanogr. 25, 329–347.
Saunders, P.M., King, B.A., 1995b. Oceanic fluxes on the WOCE A11 section. J. Phys. Oceanogr. 25, 1942–1958.
Saunders, P.M., et al. (Eds.), 1993. RRS Discovery Cruise 199, 22 Dec 1992–01 Feb 1993, WOCE A11 in the South Atlantic, in IOSDL. Cruise Report No. 234, 69pp.
Smith, W.H.F., Sandwell, D.T., 1994. Bathymetric prediction from dense satellite altimetry and sparse shipboard bathymetry. J. Geophys. Res. 99, 21803.
Smythe-Wright, D., Boswell, S., 1998. Abyssal circulation in the Argentine Basin. J. Geophys. Res. 103, 15845–15851.
Tai, C.-K., Fu, L.-L., 2005. The 25-day-period large-scale oscillations in the Argentine Basin revisited. J. Phys. Oceanogr. 35, 1473–1479.
Volkov, D.L., Fu, L.-L., 2008. The role of vorticity fluxes in the dynamics of the Zapiola Anticyclone. J. Geophys. Res. 113, C11015.
Weatherly, G.L., 1993. On deep-current and hydrographic observations from a mudwave region and elsewhere in the Argentine Basin. Deep-Sea Res. Part II: Top. Stud. Oceanogr. 40 (4–5), 939–961.
Whitworth, T., Nowlin, W.D., Pillsbury, R.D., Moore, M.I., Weiss, R.F., 1991. Observations of the Antarctic Circumpolar Current and deep boundary current in the southwest Atlantic. J. Geophys. Res. 96, 15105–15118.